PAPER

Second-harmonic interference imaging of ferroelectric domains through a scanning microscope

To cite this article: Xiaoyang Huang *et al* 2017 *J. Phys. D: Appl. Phys.* **50** 485105

View the article online for updates and enhancements.

Related content

- Superposed second-harmonic Talbot self-image from a PPLT crystal
  Dunzhao Wei, Dongmei Liu, Xiaopeng Hu et al.

- The modulation to Cerenkov second-harmonic in a LiTaO3 waveguide with annular poling domain
  C D Chen and X P Hu

- Cerenkov second-harmonic arc from a hexagonally poled LiTaO3 planar waveguide
  Yong Zhang, X P Hu, G Zhao et al.

Second-harmonic interference imaging of ferroelectric domains through a scanning microscope

Xiaoyang Huang[1], **Dunzhao Wei**[1], **Yongmei Wang**[1], **Yunzhi Zhu**[1],
Yong Zhang[1] ⬤, **X P Hu**[1], **S N Zhu**[1] **and Min Xiao**[1,2]

[1] National Laboratory of Solid State Microstructures, School of Physics, and College of Engineering and Applied Sciences, Nanjing University, Nanjing 210093, People's Republic of China
[2] Department of Physics, University of Arkansas, Fayetteville, AR 72701, United States of America

E-mail: zhangyong@nju.edu.cn (YZ) and mxiao@uark.edu (MX)

CrossMark

Abstract

We report a second-harmonic (SH) interference imaging technique to observe the ferroelectric domains of a periodically poled $LiTaO_3$ crystal through a scanning microscope. By interfering with the reference SH field, which is produced in an un-poled $LiTaO_3$ crystal, the SH imaging of the positive and negative domains can be easily distinguished. The image quality can be tuned by rotating the reference crystal or moving the focal plane. Our SH interference configuration is compatible with commercial scanning microscopy and has potential applications in fast examination of the ferroelectric structures in waveguide, film, and integrated devices.

Keywords: second-harmonic generation, ferroelectric domains, scanning microscopy

(Some figures may appear in colour only in the online journal)

1. Introduction

In recent years, increasing attention has been paid to periodically poled ferroelectric domain structures because of their attractive nonlinear optical properties. The second-order nonlinear coefficients of the inverted domains have different signs; thus, the periodical nonlinear coefficients enable quasi-phase-matching techniques for efficient frequency conversion in both one- and two-dimensional structures [1–5]. In addition, this class of materials provides more possibilities for the discovery of novel phenomena, such as conical second-harmonic generation (SHG) [6, 7], nonlinear Airy beams [8], Cerenkov second-harmonic generation [9–11], the nonlinear Talbot effect [12, 13], and superfocusing [14]. During the development of new materials, thin films of periodically inverted domains have been fabricated [15–19] that retain the ability of quasi-phase-matching of bulk structures; furthermore, as potential building blocks for integrated devices, thin films would have advantages in many applications, such as miniaturization, ease of tuning [16], and tight mode confinement [17, 18].

To monitor the poling processes and visualize the domain structures, various observation techniques for domains or domain walls have been proposed, including surface treatment [20–22], scanning electron microscopy [23], near-field scanning optical microscopy [24], scanning second-harmonic microscopy [25], electro-optic imaging [26, 27], x-ray imaging [28], and second-harmonic imaging [29]. The limitation is that these methods cannot distinguish between the antiparallel poling directions of domains noninvasively. One way to overcome this limitation is to utilize a near-field piezoelectric force microscopy, which is based on the reverse piezoelectric effect [30]. Another way is to use the far-field second-harmonic interference imaging. Under the excitation of the same fundamental field, the SH signals generated from inverted domains [25] possess different phase information because of the different signs of the second-order nonlinear coefficients. Therefore, by measuring the phase of the SH signals, the domain inversion can be observed. The phase difference of the SH can be visualized by making use of interference with an external reference field at the same frequency
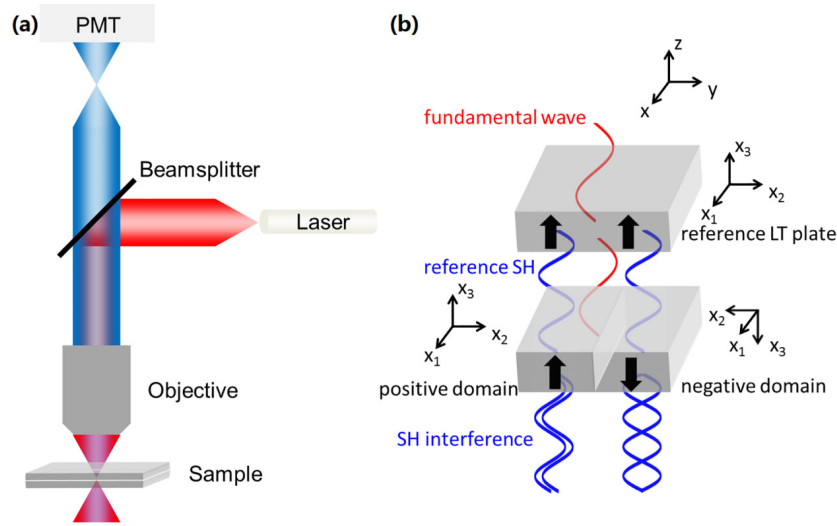
Figure 1. (a) Schematic of the scanning microscopy. (b) Visualization of inverted domains by SH interference. (x, y, z) are the space axes, (x_1, x_2, x_3) are the orthogonal physical axes of the reference LT plate and the PPLT. The thick arrows indicate the ferroelectric polarization directions.

[31–35]. Superposed SH imaging of a periodically poled LiTaO$_3$ (PPLT) plate has been obtained with transmission geometry [36], and the antiparallel domains were differentiated by bright and dark interference patterns. However, it is possible that this method does not apply to thin films because these films are usually fabricated on or bonded to substrates, which may interact with the transmitted signals. For example, the substrates may be opaque or have intrinsic nonlinearity, so they can affect the interference and imaging. In this letter, we show that the interference technique can be combined with scanning microscopy, which increases the resolution and contrast of microscope image [37]. Scanning microscopy has been widely applied in life science and material science, and here we present a convenient method based on this technique for the characterization of domain structures.

2. Experiment

Our experimental setup is illustrated in figure 1(a). We utilize a mode-locked Ti:Sapphire laser (75 fs, 80 MHz) operating at a wavelength of 840 nm as the excitation source. The fundamental wave is coupled into a commercial upright laser scanning microscope and focused onto the sample by an objective lens (40 ×, N.A. = 0.95). The sample is mounted on the stage so that the x-y plane of the crystal is horizontal, and the linearly polarized fundamental wave propagates along the z-axis. The back-reflected and scattered SH signals are collected by the same objective. Then the fundamental wave collected together is filtered out, and the SH signals are dispersed and detected by a photomultiplier.

The sample used in our experiments is a z-cut 2D PPLT plate. Domain inversion is achieved by the conventional electric poling method. The LiTaO$_3$ (LT) crystal possesses 3m symmetry, and the second-order nonlinear susceptibility can be represented as

$$[\chi_{ijk}] = \begin{bmatrix} 0 & 0 & 0 & 0 & 0 & \chi_{113} & \chi_{131} & \chi_{112} & \chi_{121} \\ \chi_{211} & \chi_{222} & 0 & \chi_{223} & \chi_{232} & 0 & 0 & 0 & 0 \\ \chi_{311} & \chi_{322} & \chi_{333} & 0 & 0 & 0 & 0 & 0 & 0 \end{bmatrix}. \quad (1)$$

Given the experimental setup, only the second-order nonlinear polarization in the x-y plane needs to be considered. Then, the second-order nonlinear polarization of the positive domains along the x- and y- directions can be written as

$$\begin{aligned} P^{2\omega}_{x,p} &= (\chi_{112} + \chi_{121})E_x E_y, \\ P^{2\omega}_{y,p} &= \chi_{211}E_x^2 + \chi_{222}E_y^2, \end{aligned} \quad (2)$$

where E_x and E_y are the fundamental fields along the x- and y- directions, respectively. The crystal structure of the negative domain can be obtained by rotating the positive domain by 180° about the x-axis; the transformation matrix of this operation is
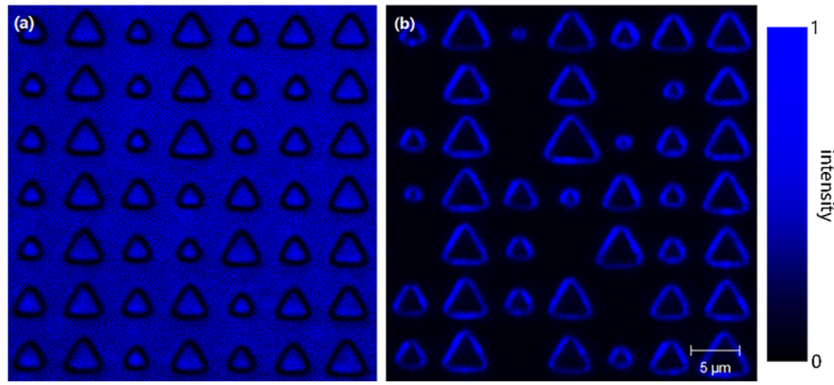
$$\alpha_x = \begin{bmatrix} 1 & 0 & 0 \\ 0 & -1 & 0 \\ 0 & 0 & -1 \end{bmatrix}. \quad (3)$$

Then, the second-order susceptibility tensor of the negative domain can be derived via the transformation

$$\chi'_{ijk} = \alpha_{il}\alpha_{jm}\alpha_{kn}\chi_{lmn}. \quad (4)$$

It is easy to see that the absolute values of all the tensor components stay unchanged after the transformation, and the signs of the non-vanishing components become negative. Therefore, the relative nonlinear polarization of the negative domains can be written as

$$\begin{aligned} P^{2\omega}_{x,n} &= (-\chi_{112} - \chi_{121})E_x E_y = -P^{2\omega}_{x,p}, \\ P^{2\omega}_{y,n} &= -\chi_{211}E_x^2 - \chi_{222}E_y^2 = -P^{2\omega}_{y,p}, \end{aligned} \quad (5)$$

J. Phys. D: Appl. Phys. **50** (2017) 485105

X Huang *et al*

Figure 2. (a) Surface SH image of the PPLT crystal without reference. (b) Cerenkov-type SHG at the domain boundaries. The image patterns present the intensity distributions of the SH waves from the samples. Scale bar, 5 μm.

and the SH signals from the positive and negative domains have a phase shift of π which can be observed by interference, as shown schematically in figure 1(b).

3. Results and discussion

Figure 2(a) shows a typical scanning SH image of the PPLT crystal without introducing the interference SH beam. Here, we locate the focal plane close to the upper surface of the PPLT sample. The dark triangular rings represent the domain boundaries among the antiparallel domains. The widths of the domain walls in figure 2(a) are measured to be 0.5 μm ~1 μm, which agree well with the reported values [38]. The second-order nonlinear coefficients in the boundaries generally become smaller because of the twisted crystal structure near the boundaries. The bright triangles and the background regions result from the positive and negative domains. The signal intensities from all of the bright areas are nearly equal because the positive and negative domains share the same absolute values of the second-order nonlinear susceptibilities, as discussed above. Also, because the Cerenkov-type SHG can be greatly enhanced by the boundaries [29], it can be utilized to observe the boundaries between the ferroelectric domains [39]. In the experiment, we increase the numerical aperture of the imaging system to collect the back-scattered Cerenkov SHG signals. As shown in figure 2(b), the bright triangular rings can be seen clearly, which result from the Cerenkov SH signals emitted at the boundaries. The areas other than the boundaries are not visualized in figure 2(b) because the Cerenkov SH signals are quite weak in homogeneous LT domains.

To study the phase information of the SH from the sample, we introduce a reference SH wave by placing a piece of *z*-cut un-poled LT crystal on top of the PPLT crystal. In this geometry, the fundamental wave travels through the LT plate first and then is transmitted into the PPLT sample, as figure 1(b) shows. Both crystals generate SH waves at the same frequency, which interfere with each other [35]. When the crystallographic axes of the reference LT crystal coincide with that of the positive domains of the PPLT crystal, their second-order nonlinear susceptibilities can be represented by the identical matrix. Therefore, the SH waves produced from the reference

crystal and the positive domains have the same phases. In this case, the positive domains are shown by constructive interference as the bright patterns in figure 3(a), while the negative domains are presented as a dark background caused by destructive interference because the corresponding SH waves have opposite phases relative to that from the reference LT crystal. The intensity pattern in figure 3(a) reflects the phases of the SH signals from various domains, which can reveal more information in comparison with the SH imaging method without the reference LT crystal [29] (see figure 2(a)). The interference SH image is obtained by scanning, i.e. only one point is recorded by the scanning microscopy at one time. In comparison with general interference microscopy [36], better resolution can be obtained. In addition, the signal-to-noise ratio can be improved because the backward signals can avoid the background SH noises in the forward direction [25]. The stable alternately bright and dark SH pattern indicates that the SH waves from antiparallel domains have different phases.

The image quality can be tuned by changing the relative phase between the reference wave and the SH from the sample, which can be achieved by simply rotating the reference LT plate around its *z*-axis by an angle of, for example, 180°. The corresponding transformation matrix is

$$
\alpha_z = \begin{bmatrix} -1 & 0 & 0 \\ 0 & -1 & 0 \\ 0 & 0 & 1 \end{bmatrix}. \tag{6}
$$

The second-order nonlinear susceptibility tensor is transformed into

$$
\begin{bmatrix} 0 & 0 & 0 & 0 & 0 & \chi_{113} & \chi_{131} & -\chi_{112} & -\chi_{121} \\ -\chi_{211} & -\chi_{222} & 0 & \chi_{223} & \chi_{232} & 0 & 0 & 0 & 0 \\ \chi_{311} & \chi_{322} & \chi_{333} & 0 & 0 & 0 & 0 & 0 & 0 \end{bmatrix}, \tag{7}
$$

and the second-order nonlinear polarization of the reference LT crystal in the *x-y* plane becomes

$$
\begin{aligned} P_{x,r}^{2\omega} &= -P_{x,p}^{2\omega} = P_{x,n}^{2\omega}, \\ P_{y,r}^{2\omega} &= -P_{y,p}^{2\omega} = P_{y,n}^{2\omega}. \end{aligned} \tag{8}
$$

The phase of the reference SH wave is shifted by π [35], while the phase of the SH waves from the PPLT domains are not
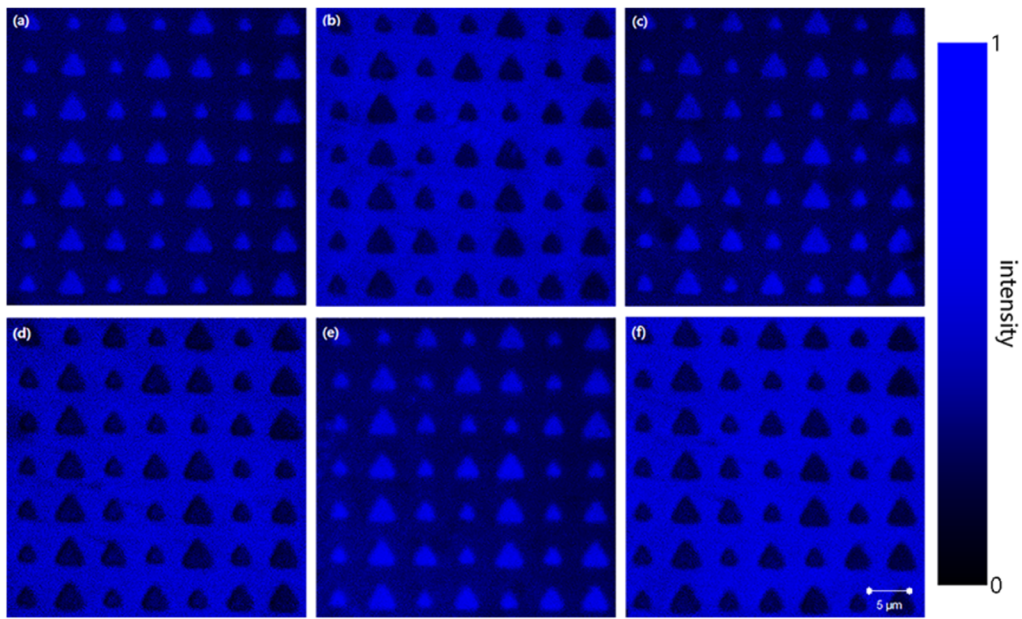
Figure 3. Superposed SH images. (a) Interference pattern when the crystallographic axes of the reference LT plate coincide with that of the positive domains. (b)–(f) Patterns under the rotation of the LT plate around the z-axis by 60°, 120°, 180°, 240°, and 300°, respectively. Scale bar, 5 μm.
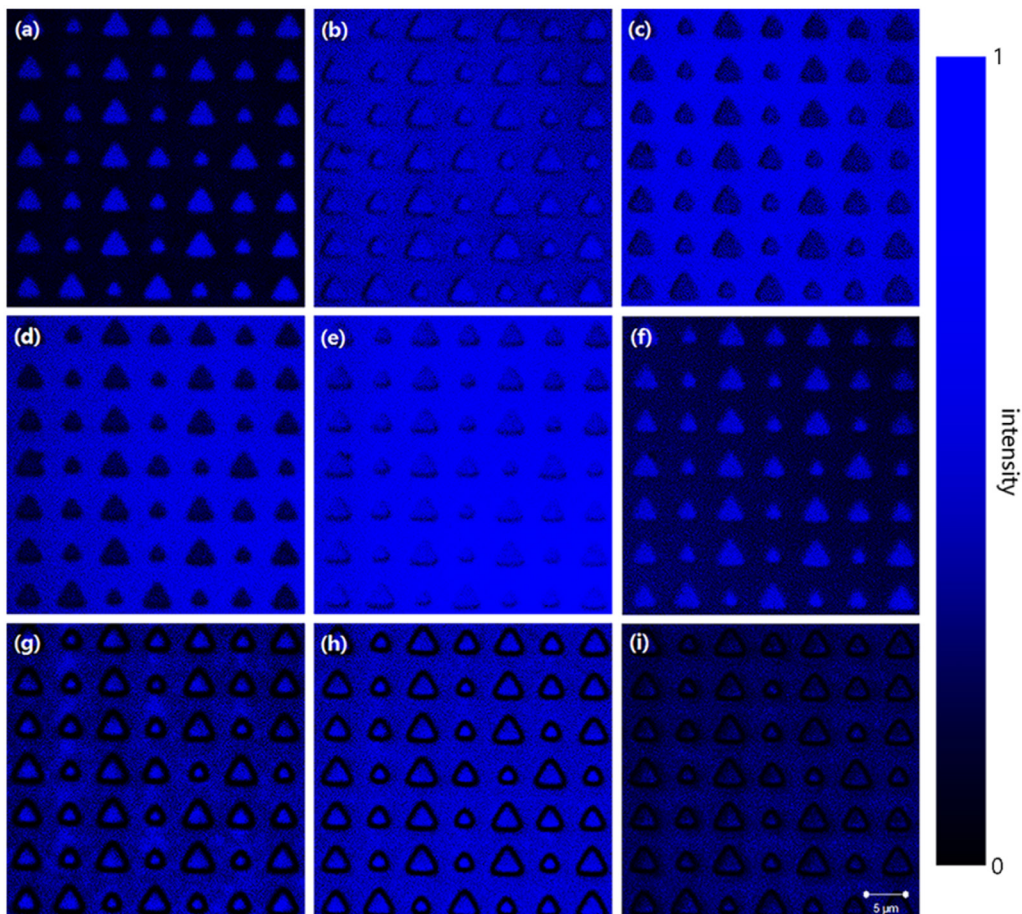
Figure 4. Images at different focal planes. From the left column to the right column, the focus moves deeper into the sample. (a)–(c) Superposed SH images at different focal planes when the crystallographic axes of the reference LT plate coincide with that of the positive domains. (d)–(f) Superposed SH images at different focal planes after the LT plate is rotated by 60°. (g)–(i) SH images without reference SH at various focal planes. Scale bar, 5 μm.

affected. Under this condition, positive domains are represented as dark triangles because of destructive interference, while the SH pattern from the negative domains is bright because of constructive interference (figure 3(d)). Because the z-axis of the LT crystal is a three-fold rotation axis, the same phase shift of π to the reference SH wave can be introduced by rotating the LT plate around the z-axis by an angle of 60° or 300°. As shown in figure 3, the interference patterns show positive domains when the LT crystal is rotated by 0° (figure 3(a)), 120° (figure 3(c)), and 240° (figure 3(e)), while the patterns with the reference LT crystal being rotated by 60° (figure 3(b)), 180° (figure 3(d)), and 300° (figure 3(f)) present negative domains. Therefore, the selective imaging of positive or negative domains in the sample can be easily achieved by rotating the reference LT plate.

In addition, the interference patterns also change with the location of the focal plane. By adjusting the position of the microscope stage along the z-axis, we visualize different planes inside the sample, as shown in figures 4(a)–(f). At the beginning, when the focal plane is at the surface of the PPLT sample, the positive domains are shown as bright triangles, while the dark background represents negative domains (figure 4(a)). As the focal plane moves deeper, the intensities of the signals from the positive domains appear to be lower first (figures 4(b)–(c)), and then increase after reaching a minimum value. Similarly, the intensities of the signals from the negative domains increase first and then decrease after reaching a maximum value. After rotating the reference LT plate by 60°, the evolution of the interference images at different imaging planes still has similar characteristics, as shown in figures 4(d)–(f). This can be attributed to an additional phase offset caused by dispersion [40]. The SH signals are mostly limited to the focal plane [25]. Before reaching the focal plane, the reference SH wave, together with the fundamental wave, propagates in the PPLT crystal for a certain distance. Because the refractive indices of waves at the fundamental and SH frequencies are different, an additional phase difference is introduced between the reference SH wave and the fundamental wave, as well as the SH wave from the PPLT crystal. The deeper the focal plane is located, the larger the phase difference is. As a result, the contrast in the SH pattern of positive and negative domains changes with the location of the focal plane. As a comparison, we study the image variation at different planes without introducing the reference SH wave. Although the intensities of SH signals vary with the location of the focal plane, they remain independent of the ferroelectric polarization of domains, as figures 4(g)–(i) show. The dependence of the superposed SH image on the depth of the focal planes provide more evidence that the periodic patterns originate from the interference between SH waves from the reference LT crystal and the PPLT crystal.

4. Conclusions

In summary, we have investigated the superposition of two SH waves from PPLT and un-poled LT slices with scanning microscopy. The interference patterns show that the SH waves

from inverted domains have different phases. By varying the imaging planes, the phase difference between the interfering waves can be adjusted, which results in various interference patterns. The SH interference scanning microscopy method reported in this work is suitable for the observation of thin films or the surface of domain structures. Besides the out-of-plane domains as demonstrated in our experiment, such imaging technique can be easily extended to observe the in-plane domains [18, 41] by properly choosing the reference plate. This method can provide better understanding of the phase features of various ferroelectric domains and enriches characterization tools for nonlinear optical materials.

ORCID iDs

Yong Zhang ⓘ https://orcid.org/0000-0003-1158-2248

References

[1] Magel G A, Fejer M M and Byer R L 1990 Quasi-phase-matched second-harmonic generation of blue light in periodically poled LiNbO₃ *Appl. Phys. Lett.* **56** 108–10

[2] Zhu S-N, Zhu Y-Y and Ming N-B 1997 Quasi-phase-matched third-harmonic generation in a quasi-periodic optical superlattice *Science* **278** 843–6

[3] Broderick N G R, Ross G W, Offerhaus H L, Richardson D J and Hanna D C 2000 Hexagonally poled lithium niobate: a two-dimensional nonlinear photonic crystal *Phys. Rev. Lett.* **84** 4345–8

[4] Ni P, Ma B, Wang X, Cheng B and Zhang D 2003 Second-harmonic generation in two-dimensional periodically poled lithium niobate using second-order quasiphase matching *Appl. Phys. Lett.* **82** 4230–2

[5] Myers L E, Miller G D, Eckardt R C, Fejer M M, Byer R L and Bosenberg W R 1995 Quasi-phase-matched 1.064 μm-pumped optical parametric oscillator in bulk periodically poled LiNbO₃ *Opt. Lett.* **20** 52–4

[6] Xu P, Ji S H, Zhu S N, Yu X Q, Sun J, Wang H T, He J L, Zhu Y Y and Ming N B 2004 Conical second harmonic generation in a two-dimensional $\chi^{(2)}$ photonic crystal: a hexagonally poled LiTaO₃ crystal *Phys. Rev. Lett.* **93** 133904

[7] Fang X, Wei D, Wang Y, Wang H, Zhang Y, Hu X, Zhu S and Xiao M 2017 Conical third-harmonic generation in a hexagonally poled LiTaO₃ crystal *Appl. Phys. Lett.* **110** 111105

[8] Ellenbogen T, Voloch-Bloch N, Ganany-Padowicz A and Arie A 2009 Nonlinear generation and manipulation of Airy beams *Nat. Photon.* **3** 395–8

[9] Kalinowski K, Roedig P, Sheng Y, Ayoub M, Imbrock J, Denz C and Krolikowski W 2012 Enhanced Čerenkov second-harmonic emission in nonlinear photonic structures *Opt. Lett.* **37** 1832–4

[10] Zhang Y, Qi Z, Wang W and Zhu S N 2006 Quasi-phase-matched Čerenkov second-harmonic generation in a

J. Phys. D: Appl. Phys. **50** (2017) 485105

X Huang *et al*

hexagonally poled LiTaO$_3$ waveguide *Appl. Phys. Lett.* **89** 171113

[11] Zhang Y, Gao Z D, Qi Z, Zhu S N and Ming N B 2008 Nonlinear Čerenkov radiation in nonlinear photonic crystal waveguides *Phys. Rev. Lett.* **100** 163904

[12] Zhang Y, Wen J, Zhu S N and Xiao M 2010 Nonlinear Talbot effect *Phys. Rev. Lett.* **104** 183901

[13] Liu D, Wei D, Zhang Y, Zou J, Hu X P, Zhu S N and Xiao M 2013 Quasi-phase-matched second-harmonic Talbot self-imaging in a 2D periodically-poled LiTaO$_3$ crystal *Opt. Express* **21** 13969–74

[14] Liu D, Zhang Y, Wen J, Chen Z, Wei D, Hu X, Zhao G, Zhu S N and Xiao M 2014 Diffraction interference induced superfocusing in nonlinear Talbot effect *Sci. Rep.* **4** 6134

[15] Radojevic A M, Levy M, Osgood R M, Jundt D H, Kumar A and Bakhru H 2000 Second-order optical nonlinearity of 10-μm-thick periodically poled LiNbO$_3$ films *Opt. Lett.* **25** 1034–6

[16] Djukic D, Cerda-Pons G, Roth R M, Osgood R M, Bakhru S and Bakhru H 2007 Electro-optically tunable second-harmonic-generation gratings in ion-exfoliated thin films of periodically poled lithium niobate *Appl. Phys. Lett.* **90** 171116

[17] Chang L, Li Y, Volet N, Wang L, Peters J and Bowers J E 2016 Thin film wavelength converters for photonic integrated circuits *Optica* **3** 531–5

[18] Mackwitz P, Rüsing M, Berth G, Widhalm A, Müller K and Zrenner A 2016 Periodic domain inversion in *x*-cut single-crystal lithium niobate thin film *Appl. Phys. Lett.* **108** 152902

[19] Shao G-H, Bai Y-H, Cui G-X, Li C, Qiu X-B, Geng D-Q, Wu D and Lu Y-Q 2016 Ferroelectric domain inversion and its stability in lithium niobate thin film on insulator with different thicknesses *AIP Adv.* **6** 075011

[20] Hooton J A and Merz W J 1955 Etch patterns and ferroelectric domains in BaTiO$_3$ single crystals *Phys. Rev.* **98** 409–13

[21] Ke C, Wang X, Hu X P, Zhu S N and Qi M 2007 Nanoparticle decoration of ferroelectric domain patterns in LiNbO$_3$ crystal *J. Appl. Phys.* **101** 064107

[22] Gao Z D, Wang Q J, Zhang Y and Zhu S N 2008 Etching study of poled lithium tantalate crystal using wet etching technique with ultrasonic assistance *Opt. Mater.* **30** 847–50

[23] Zhu S and Cao W 1997 Direct observation of ferroelectric domains in LiTaO$_3$ using environmental scanning electron microscopy *Phys. Rev. Lett.* **79** 2558–61

[24] Yang T J, Mohideen U and Gupta M C 1997 Near-field scanning optical microscopy of ferroelectric domain walls *Appl. Phys. Lett.* **71** 1960–2

[25] Flörsheimer M, Paschotta R, Kubitscheck U, Brillert C, Hofmann D, Heuer L, Schreiber G, Verbeek C, Sohler W and Fuchs H 1998 Second-harmonic imaging of ferroelectric domains in LiNbO$_3$ with micron resolution in lateral and axial directions *Appl. Phys.* B **67** 593–9

[26] Gopalan V, Gerstl S S A, Itagi A, Mitchell T E, Jia Q X, Schlesinger T E and Stancil D D 1999 Mobility of 180° domain walls in congruent LiTaO$_3$ measured using real-time electro-optic imaging microscopy *J. Appl. Phys.* **86** 1638–46

[27] Müller M, Soergel E and Buse K 2003 Visualization of ferroelectric domains with coherent light *Opt. Lett.* **28** 2515–7

[28] Kim S, Gopalan V and Steiner B 2000 Direct x-ray synchrotron imaging of strains at 180° domain walls in congruent LiNbO$_3$ and LiTaO$_3$ crystals *Appl. Phys. Lett.* **77** 2051–3

[29] Zhang Y, Wang F, Geren K, Zhu S N and Xiao M 2010 Second-harmonic imaging from a modulated domain structure *Opt. Lett.* **35** 178–80

[30] Sarid D 1994 *Scanning Force Microscopy* (New York: Oxford University Press)

[31] Fiebig M, Fröhlich D, Leute S and Pisarev R V 1998 Topography of antiferromagnetic domains using second harmonic generation with an external reference *Appl. Phys.* B **66** 265–70

[32] Hu Z H, Thomas P A, Snigirev A, Snigireva I, Souvorov A, Smith P G R, Ross G W and Teat S 1998 Phase-mapping of periodically domain-inverted LiNbO$_3$ with coherent x-rays *Nature* **392** 690–3

[33] Fiebig M, Lottermoser T, Frohlich D, Goltsev A V and Pisarev R V 2002 Observation of coupled magnetic and electric domains *Nature* **419** 818–20

[34] Van Aken B B, Rivera J-P, Schmid H and Fiebig M 2007 Observation of ferrotoroidic domains *Nature* **449** 702–5

[35] Uesu Y, Mohri H, Shindo Y and Kurimura S 2001 SHG interference microscope as a tool of nondestructive observation of ferroelectric 180° domain structures *Ferroelectrics* **253** 115–24

[36] Wei D, Liu D, Hu X, Zhang Y and Xiao M 2014 Superposed second-harmonic Talbot self-image from a PPLT crystal *Laser Phys. Lett.* **11** 095402

[37] Robert H W 1996 Confocal optical microscopy *Rep. Prog. Phys.* **59** 427

[38] Yang T J, Gopalan V, Swart P J and Mohideen U 1999 Direct observation of pinning and bowing of a single ferroelectric domain wall *Phys. Rev. Lett.* **82** 4106–9

[39] Sheng Y, Best A, Butt H-J, Krolikowski W, Arie A and Koynov K 2010 Three-dimensional ferroelectric domain visualization by Čerenkov-type second harmonic generation *Opt. Express* **18** 16539–45

[40] Bruner A, Eger D, Oron M B, Blau P, Katz M and Ruschin S 2003 Temperature-dependent Sellmeier equation for the refractive index of stoichiometric lithium tantalate *Opt. Lett.* **28** 194–6

[41] Balke N, Choudhury S, Jesse S, Huijben M, Chu Y H, Baddorf A P, Chen L Q, Ramesh R and Kalinin S V 2009 Deterministic control of ferroelastic switching in multiferroic materials *Nat. Nanotechnol.* **4** 868–75